CPM Specifications Document
Healthy Cerebral:

OSMSC 0001_0000

May 1, 2013

Version 1

Open Source Medical Software Corporation

1. Clinical Significance & Condition

Stoke is the number 4 leading cause of death in the U.S., killing more than 137,000 people a year [1]. The carotid bifurcation in the neck is the most common location of clinically significant disease. Stenosis of the proximal internal carotid artery in the carotid bulb is a major cause of stroke and hemodynamic forces are thought to play an important role in the pathogenesis of carotid atherosclerosis. Cerebral aneurysms may also form along the major arteries within the brain. If an aneurysm ruptures and subarachnoid hemorrhage occurs, risk of death is 30 to 40% and risk of severe brain damage is 20 to 30% [2]. Again, information on the hemodynamics at the major arteries deep in the brain may be important in understanding aneurysm formation.

2. Clinical Data

Patient-specific volumetric image data was obtained to create physiological models and blood flow simulations. Details of the imaging data used can be seen in Table 1. See Appendix 1 for details on image data orientation. The image data has been modified to remove patient identifying features.

Table 1 – Patient-specific volumetric image data details (mm)

OSMSC ID	Modality	Voxel Spacing			Voxel Dimensions			Physical Dimensions		
		R	A	S	R	A	S	R	A	S
0001_0000	CT	0.4883	0.4883	0.625	512	512	570	250	250	356.25

Available patient-specific clinical data collected can be seen in Table 2.

Table 2 – Available patient-specific clinical data

OSMSC ID	Age	Gender
0001_0000	30	F

3. Anatomic Model Description

Anatomic models of the vertebral arteries were created using customized SimVascular software (Simtk.org) and the image data described in Section 2. See Appendix 2 for a description of modeling methods. See Table 3 for a visual summary of the image data, paths, segmentations and solid model constructed.

Table 3 – Visual summary of image data, paths, segmentations and solid model.

OSMSC ID	Image Data	Paths	Paths and Segmentations	Model
ID: OSMSC0001 subID: 0000 Age: 30 Gender: F				

Details of anatomic models, such has number of outlets and model volume, can be seen in Table 4.

Table 4 – Anatomic Model details

OSMSC ID	Inlets	Outlets	Volume (cm^3)	Surface Area (cm^2)	Vessel Paths	2-D Segmentations
0001_0000	1	11	28.7154	178.6407	12	295

4. Physiological Model Description

In addition to the clinical data gathered for this model, several physiological assumptions were made in preparation for running the simulation. See Appendix 3 for details.

5. Simulation Parameters & Details

5. 1 Simulation Parameters

See Appendix 4 for information on the physiology and simulation specifications. Solver parameters can be seen in Table 5.

Table 5 – Solver Parameters

OSMSC ID	Time Steps per Cycle	Time Stepping Strategy
0001_0000	1200	Residual control - Min:3, Max: 5, Criteria: 0.01

5. 2 Inlet Boundary Conditions

A typical aortic waveform was prescribed to the inlet of the computational fluid dynamics (CFD) model (Figure 1). The waveform was obtained from a study by Cheng et. al., which quantified blood flow through the pulmonary circulation [3]. Since pulmonary blood flow is in series with the systemic blood flow it was assumed the amount of blood flow in the pulmonary circulation was approximately equal to that of the systemic circulation and the waveforms were similar.
See Table 6 for more inflow details.

Table 6 – Inflow details from waveforms seen in Figure 1

OSMSC ID	Period (sec)	Mean Flow (L/min)	Profile Type
0001_0000	1.2	5.07	Parabolic

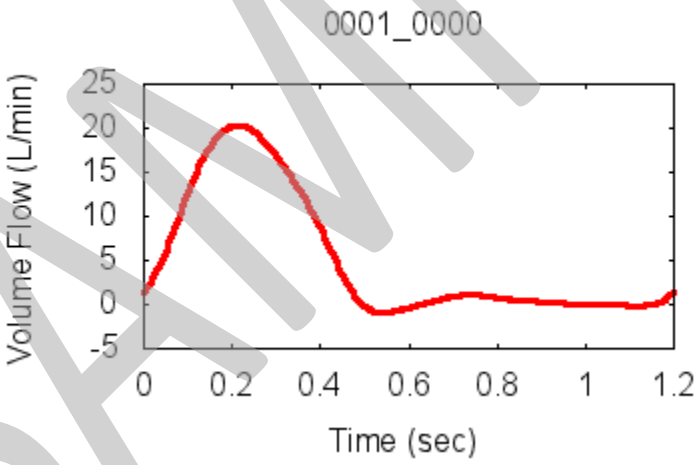

Figure 1 – Inflow waveforms in L/min

5. 3 Outlet Boundary Conditions

RCR boundary conditions were applied to each outlet. Blood flow distribution throughout the model was determined from literature. Small vessels in which flow distribution information could not be found in literature were assumed to receive negligible flow.

Descending Aorta and Subclavian Outflow

The amount of blood flow to the arteries branching off of the aortic arch was calculated based on the findings of Zamir et al., which determined the relationship between flow and diameter for the first generations of the arterial tree is regulated by the square law [4]. The diameters of the four vessels branching off of the arch were measured in the model to determine the flow to each head and neck vessel. The remaining blood flow was assumed to exit the model through the descending aorta. It was also assumed the right and left subclavian arteries received equal amounts of blood flow.

External Carotid Outflow

Marshall et al. measured the blood flow distribution of the carotid bifurcation using PC-MRI [5]. While the findings of Marshall were reported as flow rates, for the purposes of this model the flow rates were recalculated as percentages. From the blood flow in the common carotid artery (CCA), 70% of the flow was distributed to the internal carotid artery (ICA), and the 30% was distributed to the external carotid artery (ECA). As with the subclavian arteries, the flow to each ECA was assumed to be equal.

Circle of Willis Outflow

The flow distribution of the cerebral arteries was determined to be 20% to the anterior cerebral arteries (ACA), 40% to the middle cerebral arteries (MCA), and 20% to the posterior cerebral arteries (PCA) [6].

The compliance parameter of the 3-Element Windkessel model was determined based on the desired diastolic, systolic, and pulse pressure values. The total arterial compliance of the model was determined by convolving the inflow waveform with various values for Rp, Rd, and C. The ratio of Rp to the total resistance (Rp + Rd) was always chosen to be 0.056 based on the findings of Laskey et. al. [7]. After calculating a total arterial compliance that corresponded to a pulse pressure of 40 mmHg, the total arterial compliance was divided among the outlets of the model such that the compliance at the outlet was proportional to the flow.

After distributing the total arterial compliance to each outlet, the local ratio of Rp to the total resistance at each outlet was adjusted so that the desired pulse pressure was reached at each outlet. The desired pulse pressure at the subclavian and external carotid outlets was choosen to be 40 mmHg. Selecting the desired pressure values in the Circle of Willis was more complicated. Due to gravity, the blood pressure in the cerebral arteries varies depending on the posture of the subject. A subject standing in an erect posture corresponds to a static pressure difference of 20-40 mmHg between the heart and the brain [8]. Using a microcatheter, previous studies have measured the difference between cerebral and systemic blood pressure to be between 30-50 mmHg [9, 10]. For this model, the aimed pressure drop from the heart to head was chosen to be about 30 mmHg, but since gravity was not simulated a pressure drop less than 30 mmHg was expected. The pulse pressure in the cerebral vasculature was also difficult to define because of the difficulty associated with accurately measuring peak systolic and diastolic pressures using a microcatheter [11]. For the model, an *a priori* estimate of the ratio of Rp to the total resistance at each cerebral outlet was calculated assuming a pulse pressure of 40 mmHg, but with the understanding that this would likely be much less in the model.

6. Simulation Results

Simulation results were quantified for the last cardiac cycle. Paraview (Kitware, Clifton Park, NY), an open-source scientific visualization application, was used to visualize the results. A volume rendering of velocity magnitude for three time points during the cardiac cycle can be seen in Table 8 for each model.

Table 7 – Volume rendering velocity during peak systole, end systole, end diastole

ID	Peak Systole	End Systole	End Diastole
ID: OSMSC0001 subID: 0000 Age: 30 Gender: F	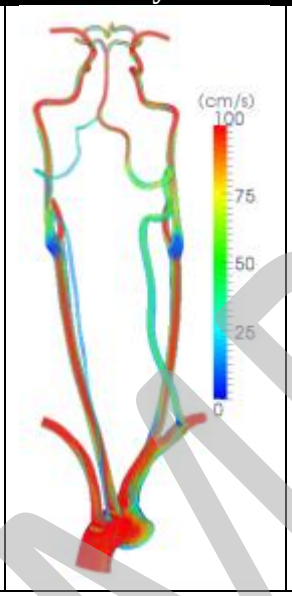	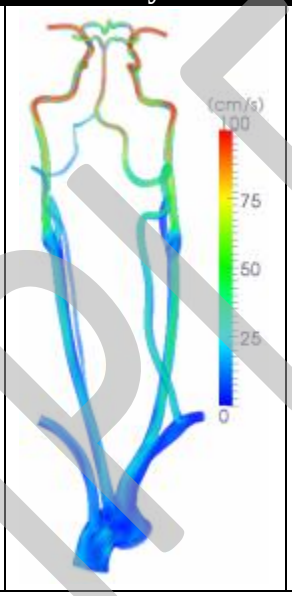	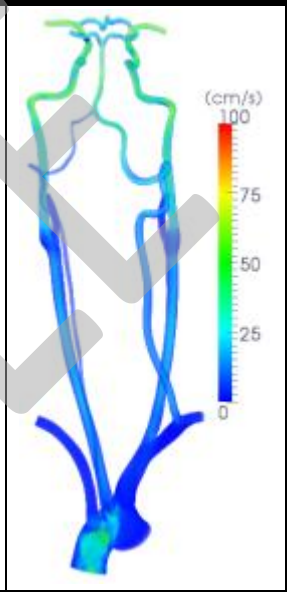

Surface distribution of time-averaged blood pressure (TABP), time-averaged wall shear stress (TAWSS) and oscillatory shear index (OSI) were also visualized and can be seen in Table 8.

Table 8 – Time averaged blood pressure (TABP), time-average wall shear stress (TAWSS), and oscillatory shear index (OSI) surface distributions

OSMSC ID	Time Averaged Pressure	TAWSS	OSI
ID: OSMSC0001 subID: 0000 Age: 30 Gender: F	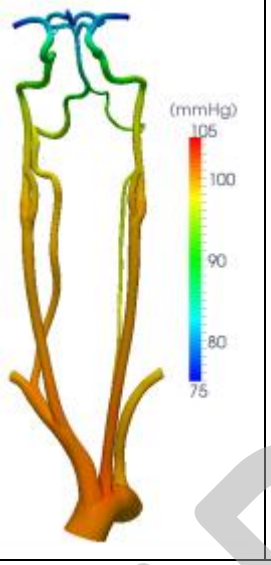	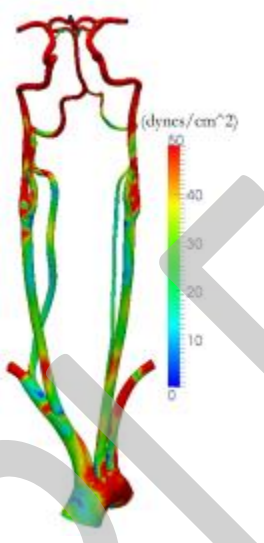	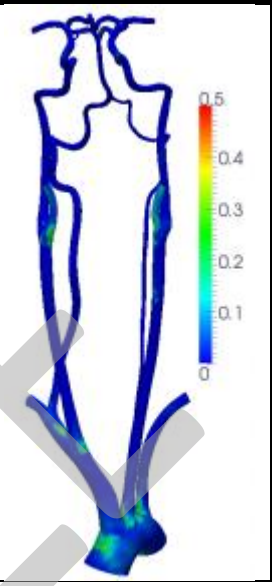

7. References

[1] American Stroke Association, "Impact of," 6 March 2012. [Online]. Available: http://www.strokeassociation.org/STROKEORG/AboutStroke/Impact-of-Stroke_UCM_310728_Article.jsp#.T3tvM6t8B8E. [Accessed 3 April 2012].

[2] American Stroke Association, "What You Should Know About Cerebral Aneurysms," 22 June 2011. [Online]. Available: http://www.strokeassociation.org/STROKEORG/AboutStroke/TypesofStroke/What-You-Should-Know-About-Cerebral-Aneurysms_UCM_310103_Article.jsp#.T3tweqt8B8E. [Accessed 3 April 2012].

[3] C. Cheng, R. Herfkens, A. Lightner, C. Taylor and J. Feisntein, "Blood flow conditionsi nt he proximal pulmonary arteries and vena cacae: healthy children during upright cycling exercise," *Am J Physiol Health Circ Physiol,* vol. 287, no. 2, pp. H921-6, 2004.

[4] M. Zami, P. Sinclair and T. Wonnacott, "Relation between diameter and flow in major branches of the arch of the aorta," *J Biomech.,* vol. 25, no. 11, pp. 1303-10, 1992.

[5] I. Marshall, P. Papathanasopoulou and K. Wartolowska, "Carotid flow rates and flow division at the bifurcation in healthy volunteers," *Physiol Meas,* vol. 25, no. 3, pp. 691-7, 2044.

[6] H. Tanaka, N. Fujita and T. Enoki et. al., "Relationship between variations in the circle of Willis and flow rates in internal carotid and basilar arteries determined by means of magnetic resonance imaging with

semiautomated lumen segmentation: reference data from 125 healthy volunteers," *AJNR Am J Neuroradiol,* vol. 27, no. 8, pp. 1770-5, 2006.

[7] W. Laskey, H. Parker, V. Ferrari, W. Kussmaul and A. Noordergraaf, "Estimation of total systemic arterial compliance in humans," *J Appl Physiol,* vol. 69, no. 1, pp. 112-9, 1990.

[8] C. Kim, C. Kiris, D. Kwak and T. David, "Numerical simulation of local blood flow in the carotid and cerebral arteries under altered gravity," *J Biomech Eng,* vol. 128, no. 2, pp. 194-202, 2006.

[9] H. Henkes, T. Gotwald, S. Brew, E. Miloslavski, F. Kämmerer and D. Kühne, "Intravascular pressure measurements in feeding pedicles of brain arteriovenous malformations," *Neuroradiology,* vol. 48, no. 3, pp. 182-9, 2006.

[10] L. Fleischer, W. Young and J. Pile-Spellman et. al., "Relationship of transcranial Doppler flow velocities and arteriovenous malformation feeding artery pressures," *Stroke,* vol. 24, no. 12, pp. 1897-902, 1993.

[11] H. Henkes, S. Felber and K. Wentz et. al., "Accuracy of intravascular microcatheter pressure measurements: an experimental study," *Br J Radiol,* vol. 72, no. 857, pp. 448-51, 1999.

Exhibit 1: Simulation Resistance Values

Table 9 – RCR Values for 0001_0000 in cgs units

ID	Face Name	Rp	C	Rd
2	D_aorta	109	1.15E-03	2316
3	R_sbclvn	1117	1.40E-04	18836
4	L_sbclvn	1287	1.40E-04	18509
5	R_ECA	3110	4.15E-05	63065
6	L_ECA	2308	4.15E-05	63626
7	R_PCA	6194	2.84E-05	71236
8	L_PCA	6202	2.84E-05	71321
9	R_MCA	2010	8.50E-05	23117
10	L_MCA	1991	8.50E-05	22899
11	R_ACA	6185	2.84E-05	71131
12	L_ACA	6026	2.84E-05	69298

Appendix

1. Image Data Orientation

The RAS coordinate system was assumed for the image data orientation. Voxel Spacing, voxel dimensions, and physical dimensions are provided in the Right-Left (R), Anterior-Posterior (A), and Superior-Inferior (S) direction in all specification documents unless otherwise specified.

2. Model Construction

All anatomic models were constructed in RAS Space. The models are generated by selecting centerline paths along the vessels, creating 2D segmentations along each of these paths, and then lofting the segmentations together to create a solid model. A separate solid model was created for each vessel and Boolean addition was used to generate a single model representing the complete anatomic model. The vessel junctions were then blended to create a smoothed model.

3. Physiological Assumptions

Newtonian fluid behavior is assumed with standard physiological properties. Blood viscosity and density are given below in units used to input directly into the solver.

Blood Viscosity: 0.04 g/cm•s^2
Blood Density: 1.06 g/cm^3

4. Simulation Parameters

Conservation of mass and Navier-Stokes equations were solved using 3D finite element methods assuming rigid and non-slip walls. All simulations were ran in cgs units and ran for several cardiac cycles to allow the flow rate and pressure fields to stabilize.

5. Outlet Boundary Conditions

5.1 Resistance Methods

Resistances values can be applied to the outlets to direct flow and pressure gradients. Total resistance for the model is calculated using relationships of the flow and pressure of the model. Total resistance is than distributed amongst the outlets using an inverse relationship of outlet area and the assumption that the outlets act in parallel.

5.2 Windkessel Model

In order to represent the effects of vessels distal to the CFD model, a three-element Windkessel model can be applied at each outlet. This model consists of proximal resistance (R_p), capacitance (C), and distal resistance (R_d) representing the resistance of the proximal vessels, the capacitance of the proximal vessels, and the resistance of the distal vessels downstream of each outlet, respectively (Figure 1).

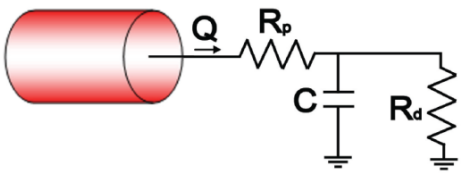

Figure 2 - Windkessel model

First, total arterial capacitance (TAC) was calculated using inflow and blood pressure. The TAC was then distributed among the outlets based on the blood flow distributions. Next, total resistance (R_t) was calculated for each outlet using mean blood pressure and PC-MRI or calculated target flow ($R_t=P_{mean}/Q_{desired}$). Given that $R_t=R_p+R_d$, total resistance was distributed between R_p and R_d adjusting the R_p to R_t ratio for each outlet.